

Debiasing Central Fixation Confounds Reveals a Peripheral “Sweet Spot” for Human-like Scanpaths in Hard-Attention Vision

Pengcheng Pan¹, Yonekura Shogo¹ & Yasuo Kuniyoshi¹

¹Department of Mechano-Informatics, The University of Tokyo

Abstract

Human eye movements in visual recognition reflect a balance between foveal sampling and peripheral context. Task-driven hard-attention models for vision are often evaluated by how well their scanpaths match human gaze. However, common scanpath metrics can be strongly confounded by dataset-specific center bias, especially on object-centric datasets. Using Gaze-CIFAR-10, we show that a trivial *center-fixation baseline* achieves surprisingly strong scanpath scores, approaching many learned policies. This makes standard metrics optimistic and blurs the distinction between genuine behavioral alignment and mere central tendency. We then analyze a hard-attention classifier under *constrained vision* by sweeping foveal patch size and peripheral context, revealing a *peripheral sweet spot*: only a narrow range of sensory constraints yields scanpaths that are simultaneously (i) above the center baseline after debiasing and (ii) temporally human-like in movement statistics. To address center bias, we propose **GCS** (Gaze Consistency Score), a center-debiased composite metric augmented with movement similarity. GCS uncovers a robust sweet spot at medium patch size with both foveal and peripheral vision, that is not obvious from raw scanpath metrics or accuracy alone, and also highlights a “shortcut regime” when the field-of-view becomes too large. We discuss implications for evaluating active perception on object-centric datasets and for designing gaze benchmarks that better separate behavioral alignment from center bias.

Keywords: active perception; hard attention; scanpath similarity; center bias; gaze metrics; peripheral vision

Introduction

Human visual perception is an active process. Rather than processing the entire visual field uniformly, humans rely on a foveated visual system and sequential eye movements to gather task-relevant information. Classic work by Yarbus and Yarbus, 1967 demonstrated that eye movement patterns are systematically shaped by task demands, suggesting that scanpaths can provide a window into underlying cognitive strategies.

In recent years, this idea has motivated the development of *hard-attention* models in machine vision, which explicitly select where to look at each step while performing tasks such as image classification or visual search (Ba et al., 2014; Mnih et al., 2014; Pan et al., 2026). These models offer a promising computational framework for studying perception under resource constraints. However, an open question remains: *when do the scanpaths produced by such models trained purely on the task meaningfully resemble human eye movements?*

A major challenge in answering this question lies in how scanpaths are evaluated. A wide range of metrics have

been proposed to compare fixation sequences, made available on FixaTons tools (Zanca et al., 2018), including Dynamic Time Warping (“Dynamic Time Warping,” 2007), ScanMatch (Cristino et al., 2010), Normalized Scanpath Saliency (Peters et al., 2005), and AUC-based measures originally developed for saliency evaluation (Judd et al., 2012). These metrics capture complementary aspects of scanpaths, such as temporal alignment, spatial overlap, and distributional similarity.

However, a long-standing finding in human eye-movement research complicates the interpretation: *human fixations are strongly biased toward the image center*. This **central fixation bias** has been robustly documented across free viewing and task-driven settings (Bindemann, 2010; Tatler, 2007; Tatler et al., 2011). Proposed explanations include photographer bias, experimental framing, oculomotor constraints, and learned expectations about where informative content is likely to appear (Smith & Mital, 2013). Crucially, center bias is not merely noise, it is a systematic property of many gaze datasets.

Center bias as a confound in scanpath evaluation. When center bias is strong, scanpath similarity metrics can be dominated by marginal spatial distributions rather than by genuine strategy similarity. Indeed, prior work in saliency modeling has shown that center-biased predictors can achieve high AUC and NSS scores without modeling image content (Borji, 2021; Borji & Itti, 2013). Despite this, task-driven scanpath evaluation has rarely applied explicit chance correction or strong spatial baselines.

This issue is particularly acute for object-centric datasets, where objects are frequently centered by design. In such settings, a trivial strategy that repeatedly fixates the center may appear “human-like” under standard scanpath metrics, even if it lacks meaningful temporal structure or task-driven exploration. As a result, high scanpath similarity does not necessarily imply cognitively plausible attention control.

Active vision, perceptual constraints, and strategy regimes. Classic work in psychology and neuroscience emphasizes that scanpaths depend strongly on task demands and internal goals (Yarbus & Yarbus, 1967). In cognitive robotics and AI, the active perception framework formalizes perception as an action-conditioned process (Bajcsy, 1988; Ballard, 1991), motivating models that must decide *where to look* under limited sensing.

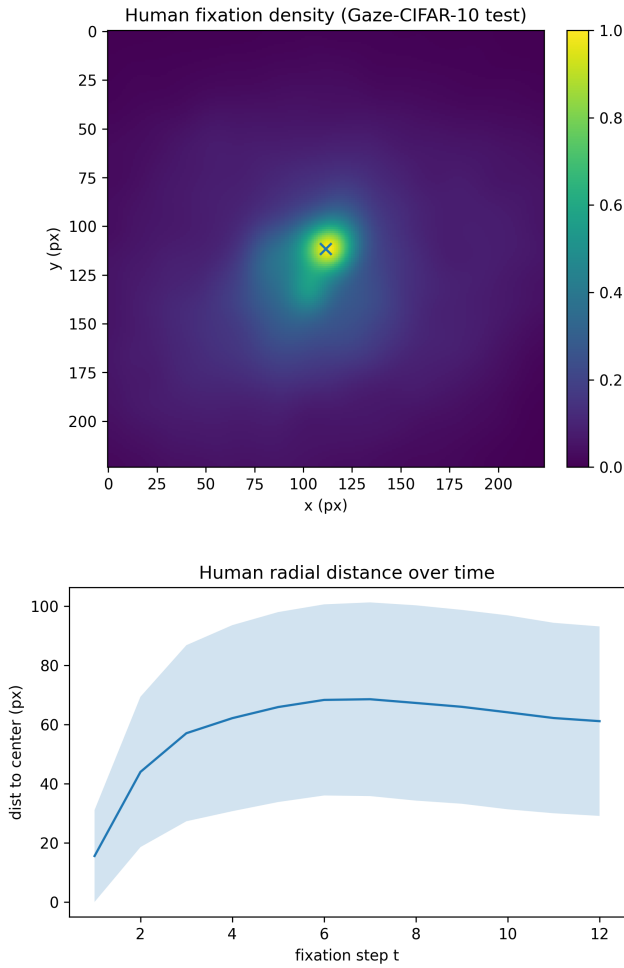


Figure 1: Human fixation density and radial distance over time (Gaze-CIFAR-10 test). The distribution is strongly center-biased, which can inflate scanpath similarity for trivial center policies.

Normative models of active vision show that optimal fixation selection depends critically on sensory constraints such as acuity, noise, and field-of-view (Geisler, 2008; Najemnik & Geisler, 2005). Manipulating these constraints can induce qualitative shifts in behavior, from exploratory search to more conservative sampling.

Similar trade-offs arise in artificial agents. Hard-attention models with access to broader spatial context can reduce the need for movement, sometimes relying on shortcut strategies that bypass sequential evidence accumulation (Geirhos et al., 2020). Conversely, overly narrow views can force excessive exploration. These observations suggest that *human-like scanpaths may emerge only within a restricted regime of perceptual constraints*.

Goals and contributions. In this work, we study these issues using Gaze-CIFAR-10 (Li et al., 2025), a gaze-annotated object recognition dataset. We make three contributions:

1. **Quantifying strong center bias in Gaze-CIFAR-10:** We provide direct empirical evidence that Gaze-CIFAR-10 exhibits strong center bias, and show that a simple center-fixation baseline achieves surprisingly high scanpath similarity under DTW, ScanMatch, NSS, and AUC.
2. **A center-debiased, movement-aware evaluation score.** We introduce **GCS** (Gaze Consistency Score), which (i) normalizes similarity using human–human agreement as an upper bound and a corner baseline as a lower bound, and (ii) explicitly subtracts a center baseline to reduce dataset-induced bias, thereby emphasizing movement dynamics beyond mere spatial overlap.
3. **Peripheral sweet spot as a mechanistic regime:** Using GCS, we reveal a *peripheral sweet spot* in a hard-attention classifier: only intermediate sensory constraints yield scanpaths that exceed the center baseline and exhibit human-like movement dynamics, whereas larger fields-of-view induce a shortcut regime.

Together, these results highlight the importance of bias-aware evaluation when using scanpaths to evaluate human-likeness, and suggest that perceptual constraints play a central role in shaping both human and artificial eye movement strategies.

Method

Gaze-CIFAR-10

We use the Gaze-CIFAR-10 dataset, which provides human fixation sequences collected during CIFAR-10 image recognition. We evaluate on the test split ($N = 9,116$ images), using the same 12 steps of fixation as the model’s glimpse steps.

Hard-Attention Classifier Under Constrained Vision

Our model is a hard-attention recurrent vision agent trained for image classification. To implement the above *constrained-vision* classifier as an *active perceiver*, we use a Multi-Level Recurrent Attention Model (MRAM), a hierarchical recurrent agent that couples *eye-movement control* with *evidence accumulation*. Conceptually, MRAM can be read as an idealized perception–action loop under partial observability: at each time step t , the agent (i) fixates, (ii) receives a limited retinal sample (a “glimpse”) determined by a *foveal patch size*, (iii) updates an internal state, and (iv) chooses where to look next.

Retina-like sensing as momentary observation. Given the current fixation location l_{t-1} , a glimpse module extracts a foveal patch (and optionally a low-resolution peripheral patch) from the image and embeds them into a fixed-dimensional sensory vector g_t . Because peripheral patches are down-sampled to the same spatial size as the foveal patch, the peripheral channel carries *wider field-of-view but lower acuity* information, whereas the foveal channel carries *higher acuity but narrower* information. This provides a simple computational analogue of the fovea–periphery trade-off familiar from human vision.

Two recurrent levels and training MRAM maintains two recurrent states updated sequentially at each time step: (1) a *lower-level* recurrent state $h_t^{(1)}$ that is driven directly by the current sensory sample g_t , and (2) a *higher-level* recurrent state $h_t^{(2)}$ that integrates information over time and supports the final decision. Intuitively, $h_t^{(1)}$ plays the role of a fast, action-oriented sensorimotor state (what to do next), whereas $h_t^{(2)}$ acts like a slower, more abstract state that accumulates evidence (what is it). This separation mirrors classic cognitive distinctions between *sampling and eye movement control* and *recognition in cortex*, and is consistent with hierarchical views of active perception in which lower circuitry drives saccade-like control while higher circuitry stabilizes task-relevant representations.

The higher-level state $h_t^{(2)}$ is mapped to a categorical prediction over labels, yielding a running belief that can be updated as new glimpses arrive. We take the final-step prediction as the agent’s classification decision after a fixed sampling budget at 12 steps, which corresponds to a bounded evidence-accumulation process. From the lower-level state $h_t^{(1)}$, a stochastic location policy samples the next fixation l_t . In our implementation, l_t is a 2D coordinate (normalized to the image plane), so the observable output is a scanpath-like sequence of fixations.

Because fixation selection is a discrete action, MRAM is trained with a REINFORCE algorithm (a Reinforcement Learning method) so that successful classifications reinforce the sampling strategies that produced informative glimpses.

Parameters to test our hypothesis. We hypothesize that *human-like scanpaths arise when the model must solve the same classification task under similar information-processing constraints as humans*. In particular, we expect human-like scanpaths to emerge most strongly under a moderately constrained field of view: if the visual input is too restricted, the agent lacks sufficient context to guide efficient sampling; if it is too broad, the task can be solved via passive, shortcut-like recognition with little need for active exploration.

We study three sensory configurations that vary peripheral context:

- **fov_only:** only a foveal patch is observed.
- **fov+per:** the agent receives both a foveal patch and a moderate low-resolution peripheral context channel.
- **big_per:** a larger peripheral context dominates the input (wider field-of-view).

The peripheral patches are down-sampled to the same size with foveal patches, thus are a low resolution window of a wider field-of-view. The foveal patches and peripheral patches are concatenated that model can learn to use either channel at the same chance. We sweep foveal patch size in $\{2, 4, 6, 8, 10, 12, 14, 16, 20, 24, 28, 32\}$ pixels, keeping the number of steps and seed fixed. Intuitively, patch size corresponds to an *effective viewing condition hypothesis*: smaller

patches require more active exploration, while larger patches allow more passive recognition.

Standard Scanpath Metrics

We report four commonly used scanpath similarity metrics: **DTW** (lower is better), **ScanMatch** (higher is better), **NSS** (higher is better), and **AUC** (higher is better).

To contextualize metric values under dataset bias, we compute three references: (i) an **upper bound** by comparing each human scanpath to itself (identical sequence), (ii) a **lower bound** using a **corner-fixation** policy, and (iii) a **center baseline** using an always-center policy.

GCS: Center-Debiased, Movement-Aware Score

We define **GCS** (*Gaze Consistency Score*) to reduce center-bias inflation. For each metric M , we normalize scores to $[0, 1]$ using the upper/lower bounds and then subtract the center baseline:

$$\tilde{D} = \frac{D_{\min} - D}{D_{\min} - D_{\max}} \quad (\text{DTW; higher is better after transform}) \quad (1)$$

$$\tilde{M} = \frac{M - M_{\min}}{M_{\max} - M_{\min}} \quad (\text{ScanMatch, NSS, AUC}) \quad (2)$$

$$\tilde{M}_{db} = \tilde{M} - \tilde{M}_{center}. \quad (3)$$

We computes a relative-error distance: $d = \sqrt{\frac{1}{K} \sum_{k=1}^K \left(\frac{|f_k^{\text{model}} - f_k^{\text{human}}|}{|f_k^{\text{human}}| + \epsilon} \right)^2}$ where f_k denotes a run-level movement statistic including total path, mean saccade amplitude, mean distance-to-center, spatial coverage, direction entropy, and collapse rate, and map it to $\text{Sim}_{move} = \exp(-d/\tau)$. Finally, we add the movement term Sim_{move} to discourage policies that match only spatial center overlap but not temporal dynamics:

$$\text{GCS} = \frac{1}{4} \sum_{M \in \{D, SM, NSS, AUC\}} \tilde{M}_{db} + \lambda \text{Sim}_{move}, \quad (4)$$

with $\lambda = 0.1$. Sensitivity analysis shows that varying λ (0 to 0.5) does not change the qualitative pattern or the sweet-spot configuration, indicating that our conclusions are driven by debiased alignment rather than a particular weighting of movement similarity. To make this confound explicit for model evaluation, we compare learned policies against the three calibration references under each metric (Figure 2). Across DTW/ScanMatch/AUC, many learned policies lie close to the center baseline, supporting the need for debiasing.

Results

Center Bias Inflates Standard Scanpath Similarity on Gaze-CIFAR-10

We first report a confound that is critical for interpreting behavioral alignment on object-centric datasets. Figure 1 shows that human fixations are strongly center-weighted over time. Consistent with this bias, Table 1 shows that a trivial center-fixation policy already attains high similarity under common

Baseline	DTW ↓	SM ↑	NSS ↑	AUC ↑
Identical-Human (upper bound)	0.003	1.000	6.052	0.995
Corner-Human (lower bound)	2023.87	0.013	-0.053	0.541
Center-Human (baseline)	702.24	0.300	1.145	0.6515

Table 1: Calibration baselines on Gaze-CIFAR-10 test. The center baseline is unexpectedly strong under standard scanpath metrics.

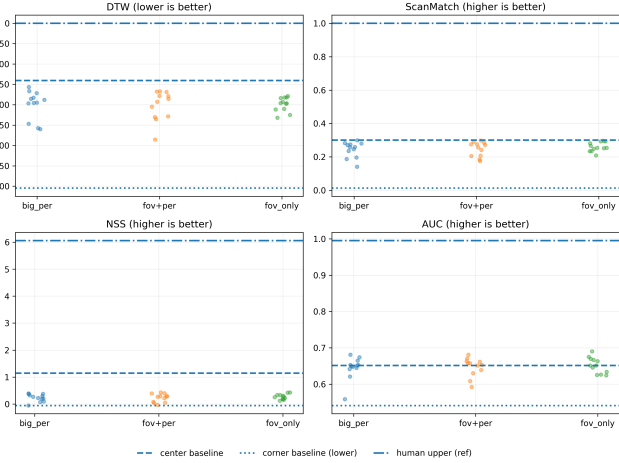


Figure 2: Raw scanpath metric distributions for three sensory settings. Dashed lines: center baseline; dotted lines: corner lower bound; dash-dot lines: human upper bound. Standard metrics can be optimistic due to center bias.

metrics. As a consequence, raw scanpath metrics can substantially overestimate alignment for policies that exploit the dataset’s center prior.

Peripheral Sweet Spot Revealed by GCS

Figure 3 shows GCS as a function of patch size under three sensory settings. Across settings, GCS identifies a clear "sweet spot" around moderate patch sizes, while too-large fields-of-view lead to degraded debiased alignment (often negative GCS). Importantly, this pattern is not obvious from accuracy alone.

The best overall alignment is achieved by **fov+per with patch size 8**:

$$\begin{aligned} \text{GCS} &= 0.0291, \quad \text{Acc} = 58.50\%, \quad \text{DTW} = 835.5, \\ \text{SM} &= 0.298, \quad \text{NSS} = 0.401 \quad \text{AUC} = 0.681. \end{aligned}$$

In contrast, the highest accuracy configuration is **fov_only with patch size 8** (Acc = 65.31%), but its GCS is much smaller (GCS = 0.0060), illustrating a non-trivial trade-off between task performance and behavioral alignment.

Table 2 summarizes key regimes, including best-GCS and best-accuracy configurations for each sensory setting, as well

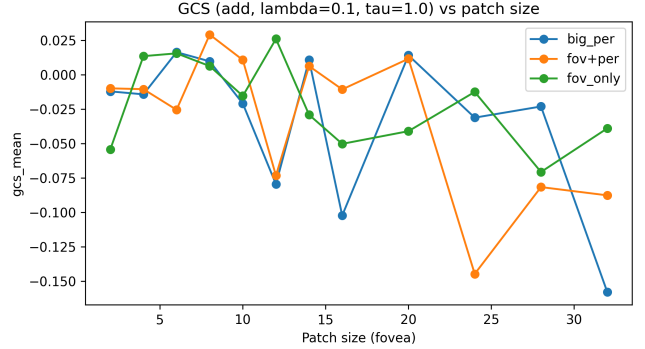


Figure 3: GCS vs. patch size for three sensory settings. GCS highlights a peripheral sweet spot (moderate constraints) and reveals degradation when the field-of-view becomes too large.

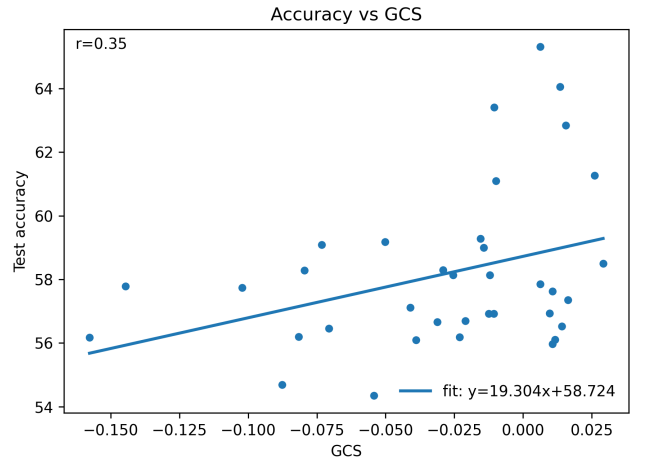


Figure 4: Accuracy vs. GCS across all runs. The correlation is modest: better recognition might imply better human scanpath alignment.

as illustrative regimes that appear strong under raw metrics. Figure 4 shows moderate correlation between recognition accuracy and scanpath similarity. In our experiments, the hard attention is trained purely on classification task, and there is no deep neural modules supporting better understanding. The modest correlation shows that artificial agent can learn to use evidences that human used for better recognition, but not necessary the same.

Movement Similarity at the Sweet Spot

A potential alternative explanation is that the sweet spot is just "more center". Movement analysis rejects this: the sweet spot is characterized by movement statistics that are closer to human trajectories, rather than simply higher central tendency.

For the best-GCS run (fov+per, ps=8), movement statistics are: model total path 190.5 vs human 429.9; mean center distance 44.3 vs 59.2; coverage 7.37 vs 10.15; direction entropy 2.42 vs 2.11; collapse rate 0.0145 vs 0.1946. These dif-

Setting	Viewport	ps	Acc(%)	DTW↓	SM↑	NSS↑	AUC↑	GCS↑	Path(px)
Best raw DTW/SM	big_per	20	56.53	783.6	0.299	0.396	0.653	0.011	123.7
Best raw AUC	fov_only	12	61.27	917.2	0.293	0.435	0.690	0.026	210.2
Best Acc	fov_only	8	65.31	986.9	0.281	0.427	0.669	0.006	329.8
Best Acc (big_per)	big_per	4	59.00	964.2	0.257	0.301	0.653	-0.015	284.3
Best Acc (fov+per)	fov+per	4	63.41	964.2	0.272	0.291	0.651	-0.010	586.4
Best GCS	fov+per	8	58.50	835.5	0.298	0.401	0.681	0.029	190.5
Best GCS (big_per)	big_per	6	57.35	857.5	0.283	0.378	0.673	0.016	158.4
Best GCS (fov_only; = Best AUC)	fov_only	12	61.27	917.2	0.293	0.435	0.690	0.026	210.2

Table 2: Key regimes illustrating the center-bias pitfall of standard scanpath metrics and the debiased composite metric (GCS). ps: foveal patch size. Path: mean total path length over 12 glimpses.

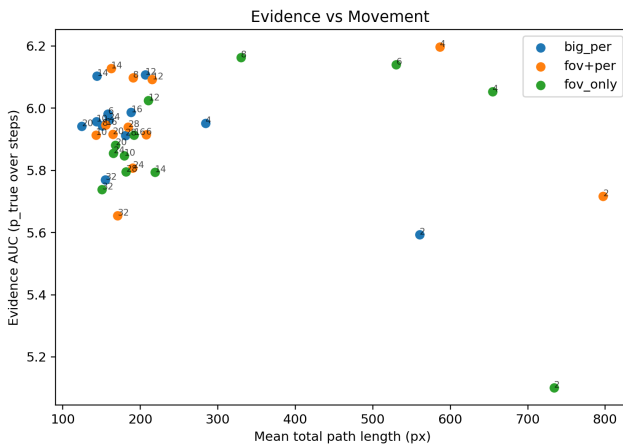


Figure 5: Evidence accumulation vs movement (per setting). The sweet spot balances active sampling and efficient evidence gain, rather than maximizing either alone.

ferences suggest the model still under-explores compared to humans, but matches several key dynamical signatures better than regimes that exploit center bias or overly large fields-of-view.

Evidence Accumulation vs Movement

To connect scanpaths to internal decision dynamics, we analyze an evidence accumulation proxy based on the probability assigned to the true class over time. Figure 5 plots evidence against total movement. We observe that regimes with very small patches move excessively (high movement without proportional evidence gain), while overly large fields-of-view reduce the need for movement (potential shortcut), weakening debiased behavioral alignment.

Discussion

Does "Human-Like" Reduce to Matching Human Viewport?

A reasonable concern is that changing patch size alters the agent’s effective viewing condition, whereas the human scanpaths were recorded under a fixed viewport. Accordingly, our results should be read as a *mechanistic regime analysis*: varying sensory constraints induces qualitatively differ-

ent exploration–decision policies, rather than simply tuning a parameter to "fit" human data.

Crucially, our claim is not that a particular patch size *matches* humans, but that three coupled observations hold: (i) widely used scanpath metrics are sufficiently center-biased that trivial center-fixation policies can obtain high scores; (ii) once we explicitly calibrate against such trivial baselines, only a narrow range of sensory configurations remains meaningfully above the center baseline; and (iii) within this regime, movement statistics become more human-like displacement patterns in ways that cannot be explained by "being centered" alone.

This perspective yields a concrete, testable prediction for future data collection. If the human viewing geometry is manipulated (e.g., viewing distance or effective image scale), human scanpaths should shift systematically across regimes that mirror our patch-size manipulation. In particular, one may observe *multiple* "sweet spots" across viewing conditions, rather than a single universal setting that defines human-likeness.

Implications for Gaze Benchmarks and Cognitive Modeling

For cognitive modeling, the results highlight a computational interpretation of gaze as *policy under sensory constraints*. For benchmark design, they caution that object-centric datasets can make scanpath evaluation deceptively easy. We advocate reporting center and corner baselines by default, and using debiased metrics such as GCS when scanpaths are used as a claim of human-likeness.

Limitations

Our experiments focus on an object-centric, low-resolution dataset and a single task in classification. Our conclusions are based on a specific hard-attention architecture and a fixed action horizon, which may constrain the diversity of emergent scanpath strategies.

Future work should test richer tasks that demand active information gathering, incorporate additional movement descriptors, and collect gaze under systematically varied viewing geometry to directly validate the proposed mechanistic regime hypothesis.

Conclusion

We showed that Gaze-CIFAR-10 exhibits strong center bias, to the extent that a trivial center-fixation baseline can achieve high scanpath similarity under common metrics such as DTW, ScanMatch, NSS, and AUC. To address this issue, we introduced GCS, a center-debiased, movement-aware evaluation score that calibrates scanpath similarity against both upper (human–human) and lower (corner) bounds and explicitly subtracts a center baseline. Using GCS, we uncovered a *peripheral sweet spot* in a hard-attention classifier: only intermediate sensory constraints yield scanpaths that reliably exceed the center baseline and display more human-like movement dynamics, whereas larger fields-of-view tend to induce shortcut regimes. Overall, our findings highlight that claims of "human-like" scanpaths require bias-aware calibration against trivial baselines and explicit consideration of movement dynamics, especially on object-centric datasets.

Acknowledgments

We acknowledge the use of AI tools for language editing and draft refinement; all analyses, results, and claims were verified by the authors. This work was supported by the JST SPRING GX Program (Grant Number JPMJSP2108). We thank Prof. Hirokazu Takahashi for insightful discussions and helpful comments that inspired this work.

References

Ba, J., Mnih, V., & Kavukcuoglu, K. (2014). Multiple object recognition with visual attention. *3rd International Conference on Learning Representations, ICLR 2015, San Diego, CA, USA, May 7-9, 2015, Conference Track Proceedings*.

Bajcsy, R. (1988). Active perception. *Proceedings of the IEEE*, 76(8), 966–1005. <https://doi.org/10.1109/5.5968>

Ballard, D. H. (1991). Animate vision. *Artificial Intelligence*, 48(1), 57–86. [https://doi.org/10.1016/0004-3702\(91\)90080-4](https://doi.org/10.1016/0004-3702(91)90080-4)

Bindemann, M. (2010). Scene and screen center bias early eye movements in scene viewing [Vision Research Reviews]. *Vision Research*, 50(23), 2577–2587. <https://doi.org/10.1016/j.visres.2010.08.016>

Borji, A. (2021). Saliency prediction in the deep learning era: Successes and limitations. *IEEE Trans. Pattern Anal. Mach. Intell.*, 43(2), 679–700. <https://doi.org/10.1109/TPAMI.2019.2935715>

Borji, A., & Itti, L. (2013). State-of-the-art in visual attention modeling. *IEEE Transactions on Pattern Analysis and Machine Intelligence*, 35, 185–207. <https://api.semanticscholar.org/CorpusID:641747>

Cristino, F., Mathôt, S., Theeuwes, J., & Gilchrist, I. (2010). Scanmatch: A novel method for comparing fixation sequences. *Behavior Research Methods*, 42, 692–700.

Dynamic time warping. (2007). In *Information retrieval for music and motion* (pp. 69–84). Springer Berlin Heidelberg. https://doi.org/10.1007/978-3-540-74048-3_4

Geirhos, R., Jacobsen, J.-H., Michaelis, C., Zemel, R. S., Brendel, W., Bethge, M., & Wichmann, F. (2020). Shortcut learning in deep neural networks. *Nature Machine Intelligence*, 2, 665–673. <https://api.semanticscholar.org/CorpusID:215786368>

Geisler, W. S. (2008). Visual perception and the statistical properties of natural scenes. *Annual review of psychology*, 59, 167–92. <https://api.semanticscholar.org/CorpusID:523591>

Judd, T., Durand, F., & Torralba, A. (2012). A benchmark of computational models of saliency to predict human fixations.

Li, J., Xue, S., & Su, Y. (2025). Gaze-guided learning: Avoiding shortcut bias in visual classification. *arXiv preprint arXiv:2504.05583*.

Mnih, V., Heess, N., Graves, A., & Kavukcuoglu, K. (2014). Recurrent models of visual attention. In Z. Ghahramani, M. Welling, C. Cortes, N. D. Lawrence, & K. Q. Weinberger (Eds.), *Nips* (pp. 2204–2212).

Najemnik, J., & Geisler, W. (2005). Optimal eye movement strategies in visual search. *Nature*, 434, 387–91. <https://doi.org/10.1038/nature03390>

Pan, P., Yonekura, S., & Kuniyoshi, Y. (2026). Emergence of fixational and saccadic movements in a multi-level recurrent attention model for vision. In T. Taniguchi, C. S. A. Leung, T. Kozuno, J. Yoshimoto, M. Mahmud, M. Dotorjeh, & K. Doya (Eds.), *Neural information processing* (pp. 299–313). Springer Nature Singapore.

Peters, R. J., Iyer, A., Itti, L., & Koch, C. (2005). Components of bottom-up gaze allocation in natural images. *Vision Research*, 45(18), 2397–2416. <https://doi.org/10.1016/j.visres.2005.03.019>

Smith, T. J., & Mital, P. K. (2013). Attentional synchrony and the influence of viewing task on gaze behavior in static and dynamic scenes. *Journal of Vision*, 13(8), 16–16. <https://doi.org/10.1167/13.8.16>

Tatler, B. W. (2007). The central fixation bias in scene viewing: Selecting an optimal viewing position independently of motor biases and image feature distributions. *Journal of Vision*, 7(14), 4–4. <https://doi.org/10.1167/7.14.4>

Tatler, B. W., Hayhoe, M. M., Land, M. F., & Ballard, D. H. (2011). Eye guidance in natural vision: Reinterpreting salience. *Journal of Vision*, 11(5), 5–5. <https://doi.org/10.1167/11.5.5>

Yarbus, A. L., & Yarbus, A. L. (1967). Eye movements during perception of moving objects. *Eye Movements and Vision*, 159–170.

Zanca, D., Serchi, V., Piu, P., Rosini, F., & Rufa, A. (2018). Fixatons: A collection of human fixations datasets and metrics for scanpath similarity. <https://arxiv.org/abs/1802.02534>